Available online at www.sciencedirect.com

SciVerse ScienceDirect

journal homepage: www.elsevier.com/locate/ijrefrig

Experimental results for a novel rotary active magnetic regenerator

K. Engelbrecht [a,*], D. Eriksen [a], C.R.H. Bahl [a], R. Bjørk [a], J. Geyti [a], J.A. Lozano [a,b], K.K. Nielsen [a], F. Saxild [c], A. Smith [a], N. Pryds [a]

[a] Department of Energy Conversion and Storage, Technical University of Denmark, Frederiksborgvej 399, DK-4000 Roskilde, Denmark
[b] POLO Research Laboratories for Emerging Technologies in Cooling and Thermophysics, Department of Mechanical Engineering, Federal University of Santa Catarina, Florianópolis, SC 88040-900, Brazil
[c] Department of Physics, Technical University of Denmark DTU Risø Campus, Frederiksborgvej 399, DK-4000 Roskilde, Denmark

ARTICLE INFO

Article history:
Received 10 February 2012
Received in revised form
3 May 2012
Accepted 4 May 2012
Available online 14 May 2012

Keywords:
Magnetic refrigerator
Regenerator
Experimentation

ABSTRACT

Active magnetic regenerator (AMR) refrigerators represent an alternative to vapor compression technology and have great potential in realizing cooling devices with high efficiency, which are highly desirable for a broad range of applications. The technology relies on the magnetocaloric effect in a solid refrigerant rather than the temperature change that occurs when a gas is compressed/expanded. This paper presents the general considerations for the design and construction of a high frequency rotary AMR device. Experimental results are presented at various cooling powers for a range of operating conditions near room temperature. The device exhibited a no-load temperature span of over 25 K and can absorb a 100 W cooling load at a 20.5 K temperature span.

Régénérateur magnétique actif et rotatif alternatif innovant : résultats expérimentaux

Mots clés : Réfrigérateur magnétique ; Régénérateur ; Expérimentation

1. Introduction

Active magnetic regenerator (AMR) refrigerators are an alternative refrigeration technology that uses a solid refrigerant that has no ozone depleting potential and no direct global warming potential. Instead the technology relies on the magnetocaloric effect, a coupling between the temperature and magnetic field of a material, which is often a reversible process. Since the magnetization/demagnetization of magnetocaloric materials (MCM) is reversible, it may be used in a thermodynamic cycle to build highly efficient cooling devices.

* *Corresponding author*. Tel.: +45 46775649; fax: +45 46775858.
E-mail address: kuen@dtu.dk (K. Engelbrecht).
0140-7007/$ – see front matter
doi:10.1016/j.ijrefrig.2012.05.003

The earliest magnetic refrigerators used a one-shot demagnetization cycle with a temperature span that was limited by the adiabatic temperature change of the magnetocaloric material (MCM), which is generally less than 5 K in practical magnetic fields and near room temperature. Such a concept was used to create the first cooling device able to cool below 1 K (Giauque and MacDougall, 1933). The operating temperature span of magnetic refrigerators can be dramatically increased by using a regenerative cycle, as first demonstrated by Brown (1976). In 1982 the active magnetic regenerator (AMR) concept was introduced, in which the regeneration is achieved by the active material itself (Barclay, 1982). Since then, many new devices have been reported (Yu et al., 2010), with modern AMRs generally using permanent magnets with regenerators made of spherical particles (Zimm et al., 2006), irregular particles (Lu et al., 2005) or parallel plates (Engelbrecht et al., 2011) of magnetocaloric material (MCM).

The AMR cycle uses a heat transfer fluid to transport the heat generated or absorbed from magnetizing and demagnetizing the MCM to a hot and a cold reservoir. The AMR cycle has four basic processes: magnetization, the cold-to-hot blow, demagnetization, and the hot-to-cold blow. During magnetization, the temperature of the MCM increases, then fluid is pumped from the cold reservoir to the hot reservoir in order to reject the magnetic work to ambient (cold-to-hot blow). The regenerator is then demagnetized, causing a decrease in temperature, and a cooling load is absorbed from the cooled space by pumping fluid from the hot reservoir across the regenerator and into the cold reservoir (hot-to-cold blow). The four processes need not be discrete, and the fluid blow may coincide with magnetization/demagnetization depending on system design. The system performance is mostly a function of the MCM, heat transfer characteristics in the regenerator, applied magnetic field and cycle parameters such as operating frequency and fluid flow rate.

This paper presents the design and performance of a novel rotary AMR using a permanent magnet with fluid flow provided by a continuously operating pump and rotary valve system. The magnet volume was optimized to provide a maximum cooling power for a given magnet volume. The necessary MCM mass is reduced by operating at higher frequency, continuously utilizing the magnetic field and by reducing parasitic losses in the system. The machine is able to operate at frequencies up to 8 Hz and has produced a cooling power above 1 kW.

Several rotary AMR devices have been reported recently using Gd regenerators, which is the benchmark MCM for use in AMR devices. A rotating regenerator AMR using cylindrical permanent magnets demonstrated a maximum cooling power of 540 W over a 0.2 K span and a cooling power of 150 W at a 5.2 K temperature span (Okamura et al., 2007). The device does not rotate continuously, and the maximum frequency reported is 0.4 Hz. The regenerator was constructed of 4 kg of Gd. A device using stationary regenerator beds and a rotating permanent magnet was shown to produce a maximum cooling power of 844 W at zero temperature span and 400 W at a temperature span of 8.1 K using a 0.89 kg regenerator of Gd (Russek et al., 2010). This device operates continuously with a maximum reported operating frequency of 4.7 Hz. A rotary magnet device using a fluid displacer to distribute fluid flow operated at a no-load temperature span of 29 K and produced a cooling power of 50 W at a temperature span of 10 K using a regenerator consisting of 0.11 kg of Gd and a maximum operating frequency of 4 Hz (Tura and Rowe, 2011). This present device reports the highest operating frequency reported so far to the knowledge of the authors.

2. Active magnetic regenerator system design

The basic design of the AMR device is a ring of magnetocaloric material rotating in the gap of two concentric cylindrical magnet assemblies. The regenerator ring is divided into 24 separate regenerator beds in nylon housings. A photograph of the system is shown in Fig. 1, and the design considerations are also discussed by Bahl et al. (2011). The magnet assemblies have four poles with four low field regions separating them, thus when rotating the regenerator, each bed will successively experience high and low magnetic field regions. This means that the AMR frequency will be four times higher than the rotational frequency of the regenerator ring. The regenerator assembly is rotated relative to the stationary permanent magnet by a belt drive connected to an AC motor. The fluid control system provides heat transfer fluid flow in alternating directions synchronized with the change in magnetic field. As viscous

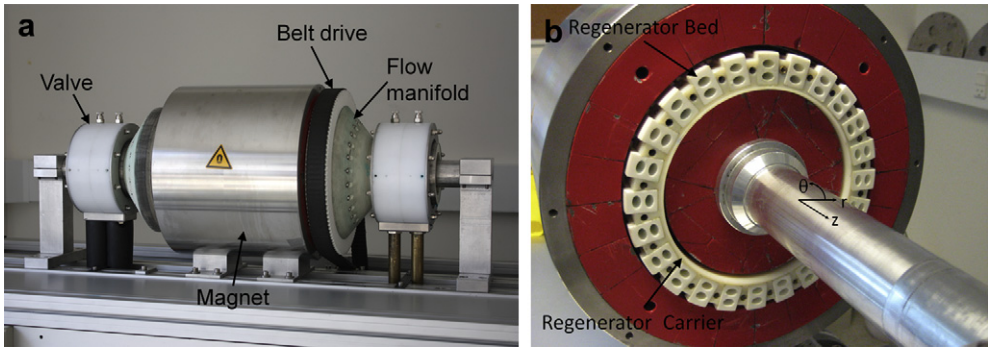

Fig. 1 – (a) A photograph of the AMR device. The regenerator assembly is located inside the cylindrical permanent magnet assemblies and the hot and cold side valve assemblies are shown. The plane where $z = 0$ is the center of the magnet (b) The regenerator assembly installed in the magnetized gap.

dissipation due to pumping losses and friction in the fluid valves can be significant system losses, the external flow system, such as connecting piping and valve interfaces, have sufficiently large flow openings as to prevent large pressure losses.

The permanent magnet provides the driver for the magnetocaloric effect and is the single most expensive component of an AMR device. It is therefore an important design consideration. The magnet design was optimized with regard to the maximum magnetic field and magnetized volume. The experimental device also has external components such as the pump, heat exchangers, and measurement devices. The main subsystems are discussed in more detail below.

2.1. *Magnet design*

The magnets used in the prototype device are based on concentric Halbach cylinder magnets, in which each cylinder is magnetized such that the remanent flux density at any point rotates continuously as the point is rotated around the z axis (Mallinson, 1973; Halbach, 1980). The number of rotations of the remanent flux density was chosen such that four high and four low field regions are created in the air gap between the magnets.

This magnet design has been optimized in order to remove unnecessary magnet material, to replace magnet material with iron where appropriate and to increase the difference in magnetic field between the high and low field regions. This resulted in a design which is segmented into 28 pieces of magnets and 8 pieces of iron. This optimization reduces the overall weight and cost of the magnet components design while increasing its efficiency. The algorithms used for these optimizations are described by Bjørk et al. (2011). A quarter of the resulting design is shown in Fig. 2a. The design of the magnet is described in more detail by Bjørk et al. (2010a).

The magnet design uses magnets with a remanence of 1.44 T. The flux density of the constructed magnet has been measured using a Hall probe (AlphaLab Inc, Model: DCM) as a function of angle, radius and length of the device and an excellent agreement between the simulated and measured flux density is seen. The measured flux density was confirmed to be periodic with a period of 90°, as expected. The measured flux density as a function of the length of the device is shown in Fig. 2b. This also shows that it is extremely important to design and model a magnet design in three dimensions, as flux will leak out of the ends of the device Bjørk (2011).

As can be seen the peak flux density is around 1.24 T while it is very close to 0 T in the low field regions. Also, the field is seen to drop off only at the very ends of the device, i.e. $|z|>100$ mm. The magnet generates a 250 mm long magnetized volume with an average flux density of 0.9 T in the four high field regions with a total volume of 2 L using 7.3 L of magnet, and has an average low flux density of 0.08 T. Finally, the working point of the magnets is very close the maximum energy density possible. The performance of the magnet can be evaluated using the Λ_{cool} parameter, which is proportional to the generated magnetic field difference to the power of 2/3, as well as the volume where the high field is generated and inversely proportional to the volume of the magnet(s) Bjørk et al. (2008). Thus a high Λ_{cool} value indicates that a high magnetic field is generated in a large volume using a small amount of magnet material. For the magnet design presented here the Λ_{cool} is equal to or better than other published magnet designs used in magnetic refrigeration devices to date (Bjørk et al., 2010b).

2.2. *Fluid control system design*

The fluid flow circuit is designed to provide continuous flow to the regenerator and to carry a net flow of heat energy from the cold reservoir (heat load) through the regenerator beds and reject it to the hot reservoir. A schematic representation of the flow circuit is given in Fig. 3. Deionized water mixed with 25% commercial ethylene glycol is used as a heat transfer fluid. Commercial automotive ethylene glycol, which includes corrosion inhibitors, was used as it has demonstrated good corrosion prevention with Gd (Engelbrecht et al., 2011). The 24 regenerator beds containing MCM are mounted on a cylinder making up the regenerator which at both ends is attached to flow heads containing fluid channels. The regenerator assembly rotates continuously and the channels in the flow

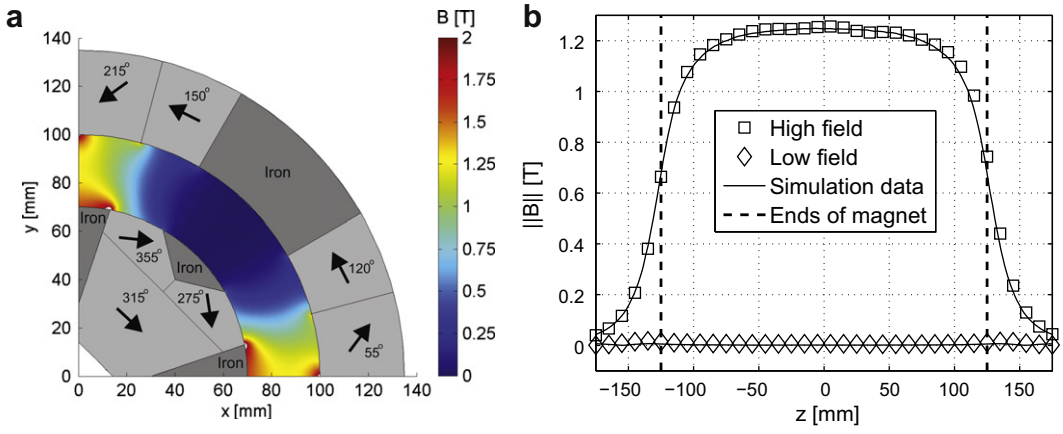

Fig. 2 – (a) A quarter of the magnet design. The magnetization is shown as black arrows on the magnets and iron is dark gray. The flux density, *B*, in the air gap is shown as a color map. (b) The flux density as a function of the position in z direction, in the middle of the air gap of the magnet at selected angles compared with numerical simulations. The figure is based on the data published by Bjørk et al. (2010a).

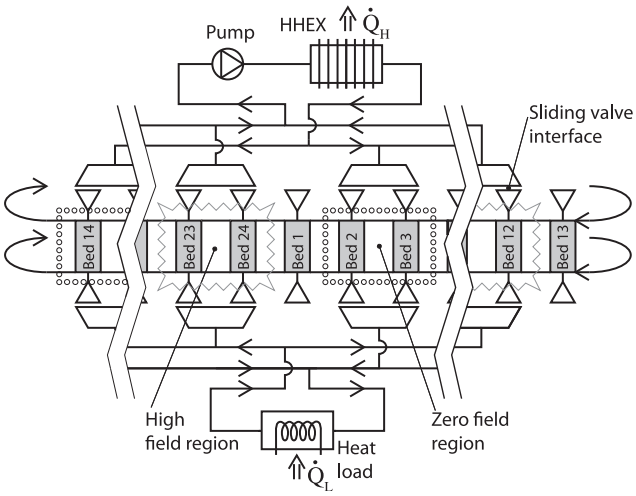

Fig. 3 – Schematic representation of the flow circuit. Here one quarter of the regenerator ring, or one magnet pole with eight regenerator beds shown, is moved past valve interfaces to the outer main flow circuit. Each bed experiences an oscillating flow as it moves through regions of high and low magnetic flux density. This schematic is repeated four times in the device, corresponding to the four magnet poles. Fluid flow is provided by a single pump. HHEX labels the hot heat exchanger.

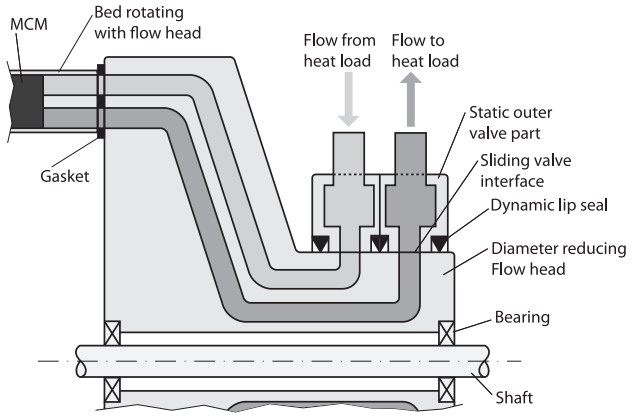

Fig. 4 – Simplified cross section view of valve/flow head system at the cold end of the regenerator. The flow head reduces the diameter from the regenerator to the valve interface leading to reduced friction losses. The fluid flow going in and out of the regenerator beds is separated into dedicated channels to avoid mixing of temperatures before and after the heat load.

heads meet the surrounding flow circuit at a valve interface. The valve interface is a contacting interface that relies on small clearances between the rotating cylinder and valve openings to prevent leakage. The valves are sealed to the outside by shaft seals. On average there are approximately eight beds that are closed to fluid flow, eight that are experiencing flow from the hot to the cold end, and eight that are experiencing flow from the cold to the hot end. The situation for each individual bed changes according to the rotation of the regenerator/flow head system in relation to the stationary magnet. The direction of flow through a bed is from hot-to-cold while in a low field region and from cold-to-hot while in a high field region.

Fig. 4 illustrates the system consisting of a rotating regenerator assembly and a static outer valve part with internal flow channels. Each bed is connected to the valve by two separate channels dedicated to flow in and out of the bed, respectively. The outer static part of the valve connects all the flow paths in each direction and it is connected to the external flow circuit. The separation of flow in dedicated channels to and from each bed eliminates dead volume, which can be a significant loss mechanism (Jacobs, 2009), and ensures that losses due to mixing of fluid at different temperatures are avoided. As indicated in Fig. 4 the diameter of the rotary valve interface is smaller than that of the regenerator. This reduction of the diameter ensures that the heat generated by the sealing friction of the rotating valve system is minimized leading to a reduction in unwanted heat dissipation to the fluid at both the hot and cold ends.

2.3. *Regenerator design and material*

The regenerator consists of a porous MCM in contact with the heat transfer fluid. The regenerator is broken into 24 regenerator beds with nylon housings. The regenerator beds are not fastened to any other component in the system and do not provide significant structural stability. Instead, the regenerator beds fit into slots on a carrier that transmits torque from the drive belt and supports the regenerator beds. In this way, the regenerator beds are captured between the fluid distributors and the regenerator carrier. This design was chosen because it allows new regenerator beds to be fabricated and installed in the machine with relative simplicity and low cost. The regenerator design also facilitates repair of individual regenerator beds.

The device described in this paper can be tested for a range of regenerator designs and materials, and the first regenerator tested was packed spheres of gadolinium. The spheres used for tests presented in this paper are 99.99% pure commercial grade Gd and were sieved to give diameters between 0.25 mm and 0.8 mm. A summary of the regenerator parameters are given in Table 1. The maximum regenerator length that the magnet can accommodate is 250 mm, although the regenerator length for the current device is 100 mm. The shorter regenerator length was chosen to reduce pressure loss in the regenerator although this reduces the utilization of the magnet. The machine is designed to be tested in the future with a parallel plate regenerator geometry with a longer regenerator.

As Fig. 1(b) shows, there is a gap between each bed of MCM. If this gap is filled with non-magnetic material, the magnetic forces acting on the regenerator assembly will be a function of the angular position in the regenerator. Since the number of regenerator beds is a multiple of the number of poles in the magnet, there will be non-equilibrium angular positions of the

Table 1 – Regenerator parameters.

Parameter	Value unit
Number of beds	24
Flow cross section (per bed)	12.5 × 19 mm^2
Length	100 mm
Regenerator volume	0.57 L
Housing material	Nylon
Material	Gadolinium
Sphere size	0.25–0.8 mm
Mass of Gd	2.8 kg

regenerator assembly caused by the varying magnetization in the regenerator. To minimize this unwanted variation in forces small blocks of iron were inserted in the gaps between regenerator beds.

For the packed sphere regenerator, the regenerator matrix is captured at both ends by a stopper with a stainless steel wire mesh screen glued to it. The spheres were allowed to pack randomly by pouring them into the regenerator housing and vibrating them. Each bed has four inlet ports: cold inlet, cold outlet, hot inlet, and hot outlet. The inlet and outlet fluid channels to each end of the bed are kept separate from the interface at the fluid valve until the fluid comes in contact with the magnetocaloric material to minimize the dead volume in each regenerator bed.

To ensure that the regenerator beds were fabricated correctly, the pressure drop in each individual bed was measured over a range of fluid flow rates and compared to the Ergun equation for flow in a packed bed (Ergun, 1952). The pressure drop can vary among beds by as much as ±20% but on average it is consistent with a packed bed of spheres with a diameter between 0.45 mm and 0.6 mm. The difference in flow resistance between the 24 beds is of concern because multiple beds are always open to fluid flow and the lower resistance beds would receive a higher share of the flow. To reduce flow channeling to lower resistance beds, the beds were arranged according to their flow resistance to minimize flow channeling between regenerator beds.

3. Experimental setup

The experimental setup allows the frequency of the AMR cycle, the fluid flow through the regenerator, the cooling load absorbed by the AMR and the hot-side reservoir temperature to be specified. For the purpose of this paper, the frequency of operation for this machine is always the AMR frequency or the number of AMR cycles per second. The motor is varied via a frequency converter and the amount of fluid flow is controlled by manually setting a bypass valve to the pump that operates at a constant flow rate. The heater power, i.e. the cooling load, is controlled by varying the voltage supplied to a resistance heater. The temperature of the hot reservoir is maintained by a counter flow heat exchanger that rejects heat to a temperature controlled bath. The temperature bath is set and the hot reservoir temperature will reach an equilibrium temperature that is a function of fluid flow rate, heat rejection rate and the heat exchanger temperature. Ambient temperature will influence system performance, as there are thermal leaks from the device to ambient. The ambient temperature is controlled by standard building HVAC and it was kept within the range of 293 K–296 K for all experiments.

The data acquisition system logs the temperature at the inlet and outlet of both the hot heat exchanger and the cold reservoir. Each measurement is taken using a type E thermocouple and a Pico Technology TC-08 Thermocouple Data Logger. The fluid flow rate is measured downstream of the heater at the cold end of the regenerator using a Burkert Type 8081 fluid flow meter. Because the valves at each end of the regenerator do not provide a positive seal, there is some leakage that will bypass the valve and return directly to the regenerator (see Fig. 4). The fluid leakage cannot be measured by the current setup and there is, therefore, some uncertainty in the actual fluid flow rate in each regenerator. The actual flow rate will be higher than the measured flow rate by the amount of leakage across the cold side valve. Fluid that bypasses the hot-side valve will return to the pump inlet and will not enter the regenerator. System pressure is measured at three locations: after the pump outlet, at the cold reservoir and at the pump inlet, by Jumo Midas Type 1001 pressure sensors. The rotational frequency of the regenerator assembly is measured by a SICK WTB4S-3P2131 Photoelectric Proximity Switch. The AMR cycle frequency is four times the rotational frequency of the regenerator assembly. Actual power consumption of the drive system, which includes frequency converter, motor and gearbox, is measured by a Elnet-Pico three-phase power multimeter located between the main electrical plug and the frequency inverter.

4. Experimental results

The resulting fluid temperatures after the system had reached steady state were measured for a range of operating conditions. For the experiments presented here, the temperature control bath temperature, which controls the hot reservoir temperature, was held constant. The machine was operated over a range of fluid flow rates, cycle frequency and cooling load. The temperature span of the device is reported as the average temperature difference between the fluid exiting the hot end of the regenerator and the fluid exiting the cold end of the regenerator. These temperatures are equivalent to those of a refrigerant entering the condenser and evaporator, respectively, in a vapor compression device.

The AMR was run with a fixed temperature bath setting and a cycle frequency of 1 Hz for varying heater loads at three different fluid flow rates, and the results are shown in Fig. 5. The hot reservoir temperature varies slightly and the range for all tests in Fig. 5 are between 300.8 K and 301.4 K. The best performance of the three tests for each cooling power was achieved with a fluid flow rate of 6.7 L min^{-1}. A temperature span of 18 K was achieved with a cooling load of 120 W.

The fluid flow rate was then held constant at 6.7 L min^{-1} and the cycle frequency was varied. The cooling power as a function of temperature span is shown in Fig. 6. The maximum temperature span produced by the AMR was found to increase with increasing frequency up to 2 Hz. At higher cooling power, the temperature span increased with

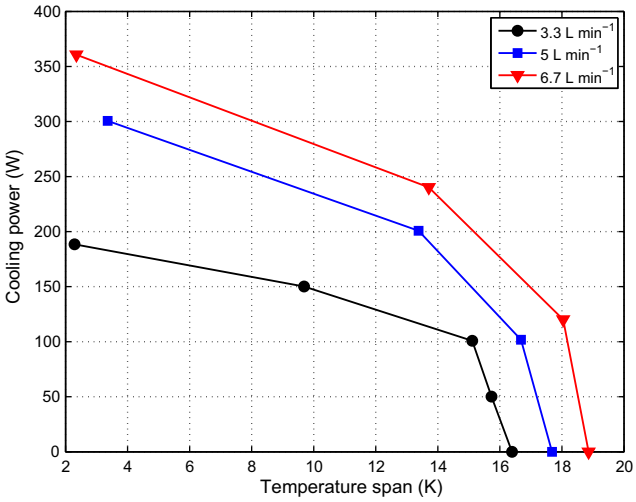

Fig. 5 – The operating temperature span of the AMR for varying cooling power at three different fluid flow rates when operating at 1 Hz.

decreasing cycle frequency. The maximum temperature span measured when a 100 W load was applied was 21 K for a 2 Hz frequency. The maximum temperature span was 24.5 K at no-load conditions and 2 Hz. System pressure increased proportionally to temperature span, due to temperature-dependent changes in viscosity. For experiments with a fluid flow of 6.7 L min^{-1}, system pressure went from 2.2 bar at high cooling load up to 3 bar when operating at its maximum temperature span.

It is possible to bypass the heater, filter and fluid flow meter in the cold end of the experimental setup and thus reduce parasitic losses to the ambient. When the cold side circuit is bypassed, the no-load temperature span increased to 25.4 K.

Experiments were also run at more extreme operating conditions to try to map out the limits of the system performance, and the results are summarized in Table 2. Results in the table show that the device is sensitive to the flow rate and hot reservoir temperature. The maximum measured cooling power was 1010 W at a 0.3 K temperature span for a fluid flow rate of 11.4 L min^{-1}.

Table 2 – Experimental results for varying fluid flow rate, cooling power and hot reservoir temperature.

Flow rate	Frequency	Hot reservoir temp.	Cooling power	Temp. span
7.6 L min^{-1}	1.8 Hz	299.9 K	324 W	8.5 K
8.3 L min^{-1}	1.8 Hz	300.1 K	498 W	2.9 K
10.0 L min^{-1}	1.5 Hz	297.9 K	400 W	13.8 K
10.4 L min^{-1}	1.8 Hz	291.8 K	746 W	3.1 K
11.4 L min^{-1}	1.8 Hz	292.3 K	1010 W	0.3 K

Finally, experiments were run at higher frequencies for a fluid flow rate of 8.3 L min^{-1}, a cooling power of 200 W and an average hot reservoir temperature of 297.5 K as shown in Fig. 7. The largest temperature span for the conditions in the figure occurred at an operating frequency of approximately 2 Hz. One explanation for the lower performance at higher frequency is that energy dissipation due to friction in the rotary valves scales with operating frequency, and the additional losses may overcome improvements in cycle performance. Operation at 2 Hz likely gives the best balance between more frequent magnetization and demagnetization of the MCM and friction losses in the rotary valve. Detailed analysis of these effects are left for another work. Another explanation could be heat transfer performance effects in the regenerator. The effect of sphere size on AMR performance has been predicted numerically by Tušek et al. (2011) and it was shown that high frequency operation requires smaller sphere diameters to achieve high performance. It may be expected that using smaller sphere diameters will produce better results in the future at high frequency.

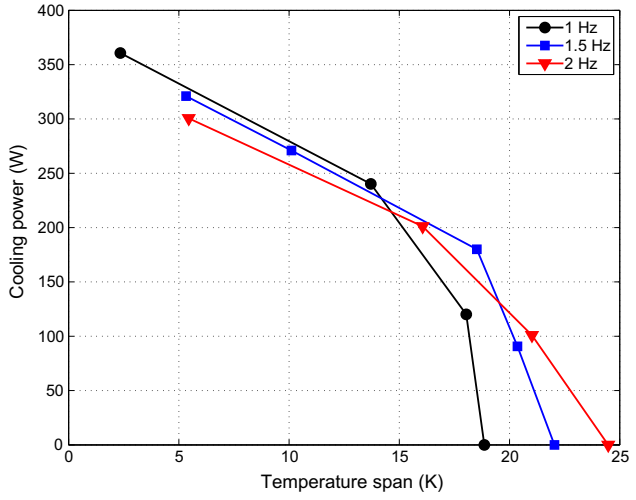

Fig. 6 – The operating temperature span of the AMR for varying cooling power when operating at three different cycle frequencies. The fluid flow rate is fixed at 6.7 L min^{-1}.

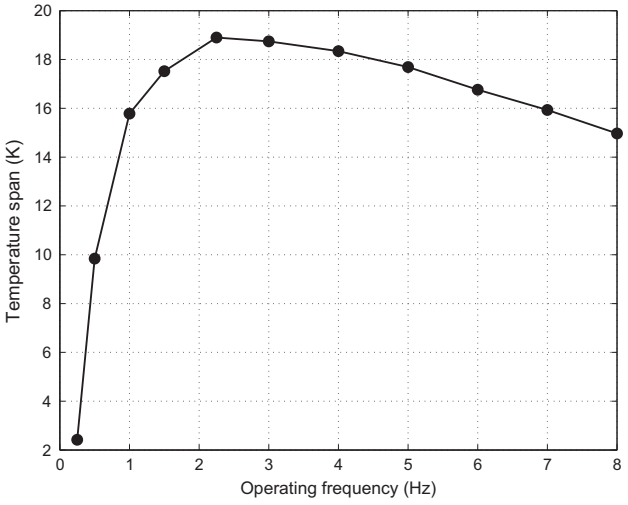

Fig. 7 – Temperature span as a function of operating frequency for a fluid flow rate of 8.3 L min^{-1} and a cooling power of 200 W.

Results for this AMR compare favorably with similar devices reported in the literature both at load and no-load conditions. The device produced the largest temperature span of any AMR in the literature known to the authors while absorbing a 100 W cooling load. However, the device uses a larger mass of MCM than reported by Russek et al. (2010) and Tura and Rowe (2011).

Power consumption of the device was measured for several of experiments reported above. The coefficient of performance, COP, is defined as

$$\mathrm{COP} = \frac{\dot{Q}_C}{\dot{W}_{motor} + \dot{W}_{pump}} \quad (1)$$

where $\dot{Q}_C$ is the cooling power, $\dot{W}_{motor}$ is the plug power used by the electric motor to rotate the regenerator and $\dot{W}_{pump}$ is the plug power used by the pump. Since a large portion of the pump flow is bypassed due to the experimental system design, the measured pump power for this setup will greatly over predict the pump power of a commercial AMR system. Therefore, the pump power is calculated according to the pressure drop and flow rate in the device,

$$\dot{W}_{pump} = \frac{\dot{V}(P_{outlet} - P_{inlet})}{\eta_{pump}} \quad (2)$$

where η_{pump} is the overall efficiency of the pump and its motor, $\dot{V}$ is the volumetric flow rate of the fluid, and P_{outlet} and P_{inlet} are the pressure at the pump outlet and pump inlet, respectively. The value of η_{pump} assumed in these calculations is 0.7, which corresponds to the overall efficiency of a properly designed pump for the application. The COP of the device operating at 1 Hz, 6.7 L min^{-1} with a cooling power of 400 W and a temperature span of 8.9 K was 1.8, while the Carnot COP is 32.4. Furthermore, at the same operational parameters but with a cooling power of 200 W and a temperature span of 15.4 K the COP was 0.8 while the Carnot efficiency is 18.3. The motor power includes inefficiencies in the motor, gear coupling and belt drive, and drag on the bearings and valves. It may be possible to significantly decrease the motor power, and thus increase COP, by redesigning the valve system and choosing a more efficient motor and transmission system.

5. Conclusions

A rotary regenerator AMR device using a stationary permanent magnet assembly has been built and was shown to produce a cooling power over a useful temperature span. The maximum observed temperature span was 25.4 K at no-load while operating at 2 Hz with a fluid flow of 6.7 L min^{-1}. The machine is able to absorb a 100 W cooling load at a temperature span of 21 K. The maximum cooling power measured was 1010 W when the machine operated at a temperature span of 0.3 K and a fluid flow rate of 11.4 L min^{-1}. A COP of 1.8 was measured for a cooling power of 400 W and a temperature span of 8.9 K.

Acknowledgments

The authors would like to acknowledge the support of the Programme Commission on Energy and Environment (EnMi) (Contract No. 2104-06–0032) which is part of the Danish Council for Strategic Research. Jaime A. Lozano thanks the financial support from CNPq (Brazil) through Grant No. 573581/2008-8 (National Institute of Science and Technology in Cooling and Thermophysics). The technical assistance of Prof. Alojz Poredoš, Dr. Samo Zupan, and Jaka Tušek is greatly appreciated.

REFERENCES

Bahl, C.R.H., Engelbrecht, K., Bjørk, R., Eriksen, D., Smith, A., Nielsen, K.K., Pryds, N., 2011. Design concepts for a continuously rotating active magnetic regenerator. Int. J. Refrigeration 34, 1792–1796.

Barclay, J.A., 1982. Use of a ferrofluid as a heat-exchange fluid in a magnetic refrigerator. J. Appl. Phys. 53, 2887–2894.

Bjørk, R., 2011. The ideal dimensions of a Halbach cylinder of finite length. J. Appl. Phys. 109 (013915)

Bjørk, R., Bahl, C.R.H., Smith, A., Christensen, D.V., Pryds, N., 2010a. An optimized magnet for magnetic refrigeration. J. Magn. Magn. Mater. 322, 3324–3328.

Bjørk, R., Bahl, C.R.H., Smith, A., Pryds, N., 2008. Optimization and improvement of Halbach cylinder design. J. Appl. Phys. 104 (1), 13910.

Bjørk, R., Bahl, C.R.H., Smith, A., Pryds, N., 2010b. Review and comparison of magnet designs for magnetic refrigeration. Int. J. Refrigeration 33 (3), 437–448.

Bjørk, R., Bahl, C.R.H., Smith, A., Pryds, N., 2011. Improving magnet designs with high and low field regions. IEEE Trans. Magn. 47 (6), 1687–1692.

Brown, G., 1976. Magnetic heat pumping near room temperature. J. Appl. Phys. 47 (8), 3673–3680.

Engelbrecht, K., Bahl, C.R.H., Nielsen, K.K., 2011. Experimental results for a magnetic refrigerator using three different types of magnetocaloric material regenerators. Int. J. Refrigeration 30 (4), 1132–1140.

Ergun, S., 1952. Fluid flow through packed columns. Chem. Eng. Prog. 48 (2), 89–94.

Giauque, W.F., MacDougall, D.P., 1933. Attainment of temperatures below 1° absolute by demagnetization of $Gd_2(SO4)_3$ $8H_2O$. Physical. Rev. 43, 768.

Halbach, K., 1980. Design of permanent multipole magnets with oriented rare earth cobalt material. Nucl. instruments Methods 169.

Jacobs, S., 2009. Modeling and Optimal Design of a Multilayer Active Magnetic Refrigeration System. Proceedings of the 3rd International Conference on Magnetic Refrigeration at Room Temperature, Des Moines, Iowa, USA, 267–274.

Lu, D.W., Xu, X.N., Wu, H.B., Jin, X., 2005. A Permanent Magnet Magneto-refrigerator Study on Using Gd/Gd-Si-Ge/Gd-Si-Ge-Ga Alloys. Proceedings of the 1st International Conference on Magnetic Refrigeration at Room Temperature, Montreux, Switzerland, 291–296.

Mallinson, J.C., 1973. One-sided fluxes - a magnetic curiosity? IEEE Trans. Magn. 9 (4), 678–682.

Okamura, T., Rachi, R., Hirano, N., Nagaya, S., 2007. Improvement of 100 W class Room Temperature Magnetic Refrigerator. Proceedings of the 2nd International Conference of Magnetic Refrigeration at Room Temperature, Portoroz, Slovenia, 377–382.

Russek, S., Auringer, J., Boeder, A., Chell, J., Jacobs, S., Zimm, C., 2010. The Performance of a Rotary Magnet Magnetic Refrigerator with Layered Beds. Proceedings of the 4th International Conference on Magnetic Refrigeration at Room Temperature, Baotou, Inner Mongolia, China, 339–349.

Tura, A., Rowe, A., 2011. Permanent magnet magnetic refrigerator design and experimental characterization. Int. J. Refrigeration 34, 628–639.

Tušek, J., Kitanovski, A., Prebil, I., Poredoš, A., 2011. Dynamic operation of an active magnetic regenerator (AMR): numerical optimization of a packed-bed AMR. Int. J. Refrigeration 34, 1507–1517.

Yu, B., Liu, M., Egolf, P.W., Kitanovski, A., 2010. A review of magnetic refrigerator and heat pump prototypes built before the year 2010. Int. J. Refrigeration 33, 1029–1060.

Zimm, C., Boeder, A., Chell, J., Sternberg, A., Fujita, A., Fujieda, S., Fukamichi, K., 2006. Design and performance of a permanent-magnet rotary refrigerator. Int. J. Refrigeration 29 (8), 1302–1306.